Available online at www.sciencedirect.com

SCIENCE DIRECT®

Materials Chemistry and Physics 83 (2004) 350–353

MATERIALS CHEMISTRY AND PHYSICS

www.elsevier.com/locate/matchemphys

# Growth and optical property of Mg, Fe co-doped near-stoichiometric $LiNbO_3$ crystal

Tao Zhang*, Biao Wang, Fu-Ri Ling, Shuang-Quan Fang, Yu-Heng Xu

*Electro-Optics Technology Center, Harbin Institute of Technology, P.O. Box 1225, Harbin 150001, PR China*

Received 21 August 2003; received in revised form 15 September 2003; accepted 24 October 2003

## Abstract

The Mg-doped and undoped, Fe near-stoichiometric $LiNbO_3$ crystals were grown from the Li-rich melt by Czochralski technique. The UV-Vis absorption spectra and infrared transmittance spectra were measured to study the structure and defects of the crystals. The photo-damage resistance ability of the crystals was characterized by observing transmission facula distortion directly. The photo-damage resistance ability of Mg (3.0 mol%):Fe (0.01 wt.%):SLN is higher than that of Fe (0.01 wt.%):SLN and Fe (0.01 wt.%):CLN. This difference is attributed to the photoconductivity increase.

*Keywords:* Near-stoichiometric $LiNbO_3$; UV-Vis absorption spectra; IR transmission spectra; Photo-damage resistance ability

## 1. Introduction

Lithium niobate ($LiNbO_3$, LN) single crystal is one of the most useful optical materials because of its potential applications, such as optical signal processing [1], imaging [2,3], holographic recording of information [4,5], and optical waveguides [6,7]. Almost all commercially available $LiNbO_3$ crystals are typical non-stoichiometric compositions, which are grown from a congruent composition melt ([Li]/[Nb] = 0.946, atomic ratio) by Czochralski technique. Although congruent $LiNbO_3$ crystals (labeled CLN) generally have good quality and uniformity, a high concentration of intrinsic defects, i.e. $Nb_{Li}$ (Nb occupied Li site) and $V_{Li}$ vacancies according to Li-site vacancy model reported by Iyi et al. [8,9], usually appear in single crystals. The near-stoichiometric crystals (labeled SLN) are thought to have superior behaviors with fewer defects because of higher Li content in crystal lattice. Thus, the improvement of optical properties in SLN crystals, i.e. faster response time [10], bigger exponential gain coefficient $\Gamma$ [11], higher sensitivity and dynamic range [12], and stronger photo-damage resistance ability [13,14], were reported compared with that of CLN crystals.

It is known that undoped congruent $LiNbO_3$ usually shows a low threshold for photorefractive damage [15]. Since Zhong et al. [16] reported the photo-damage resistance ability of $LiNbO_3$ was greatly improved with $Mg^{2+}$ impurity if more than 4.6 mol% MgO was added to the congruent composition melt, some other photo-damage resistance impurities have been discovered, such as divalent $Zn^{2+}$ [17], trivalent $In^{3+}$ [18], and $Sc^{3+}$ [19], which also suppress photorefraction and increase photo-damage resistance ability in $LiNbO_3$. Photo-damage is affected strongly by the Li/Nb ratio, and improved remarkably by a small amount of MgO doping for $LiNbO_3$ single crystals in near-stoichiometric composition [14].

In this paper, both the co-doped near-stoichiometric and congruent single crystals were grown to observe the ferroelectric domain structure. The UV-Vis absorption spectra and infrared transmittance spectra were measured to study the structure and defects of the crystals. The microscopic mechanism of photo-damage resistance ability increase in the crystals is explored.

## 2. Experimental

### 2.1. Crystal growth

The crystals were grown in our laboratory from a melt of Li-rich composition, [Li]/[Nb] = 1.38, by Czochralski technique in air atmosphere. The raw materials used to grow crystals are $Li_2CO_3$, $Nb_2O_5$, $Fe_2O_3$ and MgO with the purity

---

* Corresponding author.

*E-mail address:* zhangt02@163.com (T. Zhang).

0254-0584/$ – see front matter © 2003 Elsevier B.V. All rights reserved.
doi:10.1016/j.matchemphys.2003.10.010

Table 1
Summary of doping levels and composition for the crystals

| | No. 1 | No. 2 | No. 3 |
|---|---|---|---|
| [Li]/[Nb] starting composition | 0.946 | 1.38 | 1.38 |
| $10^3$ [$Fe_2O_3$] doping (wt.%) | 10 | 10 | 10 |
| [MgO] doping (mol%) | 0 | 0 | 3 |
| Crystal size ($mm^2$) | Ø40 × 30 | Ø24 × 28 | Ø22 × 26 |
| Wafer size ($mm^3$) | 10 × 2 × 10 | 10 × 2 × 10 | 10 × 2 × 10 |
| Appearance | Transparent | Transparent | Transparent |
| [$Li_2O$] in crystal (mol%)[a] | 48.56 | 49.60 | 48.45 |
| $10^3$ [$Fe_2O_3$] in crystal (wt.%)[b] | 9.93 | 9.77 | 9.53 |
| [MgO] in crystal (mol%)[b] | – | – | 2.12 |

[a] The $Li_2O$ concentration in crystal was calculated by the method in [20].
[b] It was measured by X-ray fluorescence analysis.

of 99.99%. The compositions and doping levels are listed in Table 1. In order to form polycrystalline bulk, the raw materials were precisely weighed, thoroughly mixed for 12 h, and fully calcined at 700 °C for 2 h and then sintered at 1150 °C for 2 h, respectively. The initial weight of the reached materials that was charged in a platinum crucible with the size of 80 mm in diameter and 50 mm in height was approximately 1000 g. The SLN crystals were pulled from the melt along the direction of [0 0 1] at a growth rate of 0.2–0.3 $mm\,h^{-1}$, the seed rotation rate was 15–20 rpm, and the axial temperature gradient above the melt surface was 30–35 $°C\,cm^{-1}$. Since the growth rate was considerably lower for the SLN versus the CLN, automatic diameter control (ADC) system was not employed during the growth of SLN.

To keep the composition homogeneity, the crystal growth was abruptly stopped when about 5 wt.% of the initial charge had pulled out, and slowly cooled down to room temperature at a rate of 80 $°C\,h^{-1}$. The typical as-growth crystal sizes of SLN (No. 2 and No. 3) were ∼20 mm in diameter and ∼30 mm in length. For comparison, Fe (0.01 wt.%):CLN crystal was also grown, and then polarized in another resistive furnace at about 1210 °C with an applied d.c. electric current density of 5 $mA\,cm^{-2}$ for 30 min at the end of the crystal growth. However, the SLN crystals were single-domain structure without polarizing treatment. The samples of the size of 10 mm × 2 mm × 10 mm ($a \times b \times c$) were cut along (0 1 0) lane from the middle of crystals, ground by using SiC powder, and then polished by using a 0.25 μm diamond solution. The crystal appearance was also listed in Table 1.

### 2.2. Measurement

The domain structure was observed by a method described elsewhere [21]. After growth, the as-growth crystals were sliced perpendicular to the growth direction, then polished. The slices were etched in a mixed acid solution ($HF:HNO_3 = 1:2$, volume ratio), then the slice surface was observed under an optical microscope.

The UV-Vis absorption spectra of the crystals were recorded by a wavelength range 300–900 nm UV-Vis spectrophotometer (CARYIE model) at room temperature. The infrared transmittance spectra of the crystals were recorded by an IR spectrophotometer (Fourier model) with the wavenumber range of 3000–4000 $cm^{-1}$ at room temperature.

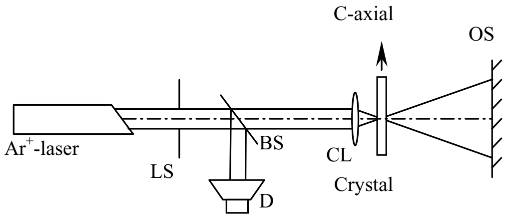

Fig. 1. Experimental setup of the photo-damage resistance ability measurement: LS, light shed; BS, beam splitter; D, detector; CL, convex lens; OS, observation screen.

The direct observing transmission facula distortion method was used to measure the photo-damage ability of these crystals. The experimental setup is shown in Fig. 1. The $Ar^+$:Laser of $\lambda = 488.0$ nm was used as light source and its light intensity was regulated by an attenuator. The beam passed through the light shed and convex lens, and then was focused on the crystal. The polarization direction of the laser beam was aligned along the *c*-axial of crystal. When the laser intensity was low, there was no photo-damage and the facula was round. As the laser beam intensity was increased gradually, the photo-damage took place in the crystal and the facula was elongated along the *c*-axial of the crystal. The threshold laser beam intensity, which initiated the facula beginning to distort, was defined as the photo-damage resistance ability of the crystal.

## 3. Results and discussion

It was observed that both doped as-growth SLN crystals (No. 2 and No. 3) without polarizing treatment shown single-domain structures under the optical microscope. Therefore, this is a big advantage because the polarizing treatment at high temperature creates cracks or scattering centers in the crystals.

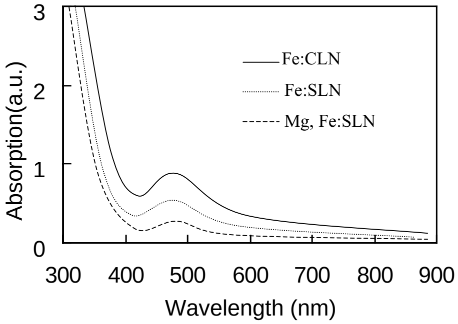

Fig. 2. The UV-Vis absorption spectra of the crystals.

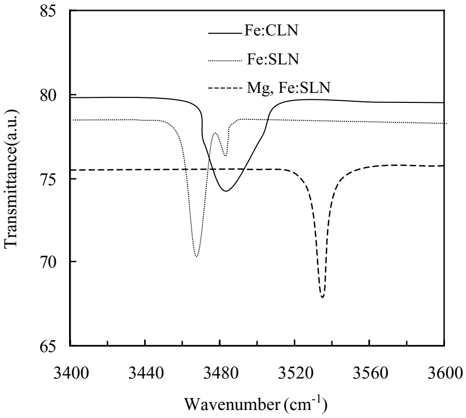

Fig. 3. The infrared absorption spectrum of the crystals.

Fig. 2 shows the UV-Vis absorption spectra of the crystals. The absorption edge of Fe:SLN shifts to ultraviolet band compared with that of Fe:CLN, while shifts to infrared band compared with that of Mg, Fe:SLN. There is a broad absorption band located at 450–520 nm, which is attributed to $Fe^{2+}$ ions absorption [22] or bipolaron absorption [23] in which the bipolarons are electrons trapped at $Nb_{Li}$ and $Nb_{Nb}$ sites. The $LiNbO_3$ crystal is oxygen octahedron structure. There are two $Nb^{5+}$, two $Li^{2+}$ and two vacancies, respectively, around every $O^{2-}$. The fundamental optical absorption edge, decided by valence electron transition energy from p states of the oxygen ions to d states of the niobium transition metal ions, is sensitive to dopants. The valence electronic state of the oxygen ions directly affects the position of the fundamental absorption edge. If impurity ions increase the polarization of the oxygen ion increase, the electron clouds distortion level will increase and result in the decrease of the energy gap. The increasing polarization causes the absorption edge shift toward the infrared band. On the contrary, it shifts to the ultraviolet band. The polarization ability values of $Li^{+}$, $Nb^{5+}$, and $Mg^{2+}$ are 2.9, 26.1, and 9.4, respectively. In Fe:SLN, there are much less intrinsic defects $Nb_{Li}$ since it has higher Li concentration than Fe:CLN (see Table 1), so the extent of $O^{2-}$ polarization is reduced, and results in its absorption edge shift towards ultraviolet band. When $Mg^{2+}$ is incorporated into lattice of Mg, Fe:SLN, a part of $Mg^{2+}$ start to enter the normal Nb sites after replacing all the anti-site $Nb_{Li}$ completely. The substitution makes the extent of $O^{2-}$ polarization decrease, and the energy gap increases. Therefore, the absorption edge of Fe:SLN, compared with that of Mg, Fe:SLN, shifts to infrared band.

Because of $H_2O$ vapor existing in atmosphere, the vapor can be introduced into crystals during the growth of crystals, which brings $H^{+}$ into crystals and forms O–H bond. The $OH^{-}$ infrared spectra are related to the circumstance around them. The position of ions can be conjectured by analyzing the change of $OH^{-}$ spectra. Fig. 3 shows the infrared transmission spectra of the crystals.

The $OH^{-}$ absorption peak of Fe:CLN is located at about 3484 cm$^{-1}$ (FWHM of about 30 cm$^{-1}$), corresponding to the vibration of $OH^{-}$–$(V_{Li})^{-}$ complex (Li-site vacancy model) [24]. The $OH^{-}$ absorption peak of Fe:SLN shifts to a narrow line at 3466 cm$^{-1}$ (FWHM less than 3 cm$^{-1}$), which is always present in nominally pure or weakly doped near-stoichiometric $LiNbO_3$. The appearance of 3535 cm$^{-1}$ sharp line of Mg:Fe:SLN indicates that the Mg content in the crystal is over the threshold. It is proposed that the Mg ions over the threshold concentration replace anti-site Nb firstly, and then the additional Mg ions entering Li and Nb sites form $(Mg_{Nb})^{3-}$–$(Mg_{Li})^{+}$ pairs. Because the pairs have a stronger force to attract $H^{+}$, the $H^{+}$ in the $OH^{-}$–$(V_{Li})^{-}$ complexes are pulled to $(Mg_{Nb})^{3-}$–$(Mg_{Li})^{+}$ pairs. Thus $(Mg_{Nb})^{3-}$–$OH^{-}$–$(Mg_{Li})^{+}$ complexes are formed, which is responsible for the absorption peak at 3535 cm$^{-1}$.

In holographic storage experiment, higher photo-damage resistance ability can improve the quality of the storage information, suppress noise generation, and reduce the bit error rate. Table 2 lists the damage resistance ability for the crystals. The results show clearly that the resistance ability of Mg (3.0 mol%):Fe (0.01 wt.%):SLN (No. 3) is higher than that of Fe (0.01 wt.%):SLN (No. 2), and is three order of magnitude higher than that of Fe (0.01 wt.%):CLN (No. 1).

It is well-known that the photorefraction can be described by the scalar expression [22] $\delta\Delta n \cong Rj_{ph}/\sigma \approx Rk\alpha I/\sigma$, where $R$ is the generalized electro-optical coefficient; $j_{ph}$ the photovoltaic current; $\sigma = \sigma_d + \sigma_{ph}$ the conductivity; $\sigma_d$ and $\sigma_{ph}$ are dark conductivity and photoconductivity, respectively; $k$ the Glass constant; $\alpha$ the optical-absorption coefficient; and $I$ the light intensity. The formula shows that increase in conductivity will decrease photorefraction. The

Table 2
Photo-damage resistance ability of the crystals

| Crystal | Photo-damage resistance ability (W cm$^{-2}$) | Photo conductivity, $\sigma_{ph}$ ($\Omega^{-1}$ cm$^{-1}$) |
|---|---|---|
| No. 1 | $1.8 \times 10^{2}$ | $8.4 \times 10^{-16}$ |
| No. 2 | $6.1 \times 10^{3}$ | $1.6 \times 10^{-15}$ |
| No. 3 | $4.0 \times 10^{5}$ | $2.7 \times 10^{-13}$ |

photoconductivity of the crystals was determined from the erasure process of the holographic gratings under light illumination [25,26], as shown in Table 2. The conductivity $\sigma_d$ can be neglected because of a long memory time in darkness. Therefore, the photorefraction is only proportional to the ratio of photovoltaic current to the photoconductivity. It is shown that the photoconductivity of No. 3 is 17 times bigger than that of No. 2, and three orders of magnitude bigger than that of No. 1. The increase in conductivity indeed decreases the photorefraction, and it is shown that the photo-damage resistance ability of No. 2 is higher with the No. 3 is the highest.

How do Mg ions affect the replacement sites of Fe ions? From the above discussion, we conclude that Mg ions substitute anti-site Nb, and then Li and Nb sites. At the same time, $Fe^{3+}$ ions occupying Li sites are pushed to the Nb sites and exist in the form of $(Fe_{Nb})^{2-}$. Because $(Fe_{Nb})^{2-}$ defects present electronegative, this makes the $Fe^{3+}$ centers loss their electron acceptor properties, and drastically reduces the capture cross-section of electrons by $Fe^{3+}$. Thus the photoconductivity increases rapidly and therefore the photorefraction decreases. So the photo-damage resistance ability of No. 3 is much higher than that of No. 2.

## 4. Conclusion

When the concentration of Mg ions exceed the threshold concentration, they replace the anti-site $Nb_{Li}$ preferentially. After the complete removal of ${Nb_{Li}}^{5+}$, $Mg^{2+}$ occupies Li and Nb sites simultaneously, and Fe ions are pushed to the Nb sites from the $Nb_{Li}$ sites. The photo-damage resistance ability of Mg (3 mol%):Fe:SLN is much higher than of Fe:SLN and Fe:CLN.

## Acknowledgements

This work was financially supported by the National Research for Fundamental Key Projects No. 973 (G19990330), the National Advanced Technology Program No. 863 (2001AA31304), the National Natural Science Foundation (10172030), and the Nature Science Foundation of Heilongjiang Province (A01-01), People's Republic of China.

## References

[1] T.Y. Chang, J.H. Jong, P. Yeh, Opt. Lett. 15 (1990) 743.
[2] Y. Fainman, E. Klancni, S.H. Lee, Opt. Eng. 25 (1986) 228.
[3] M. Cronin-Golomb, A.M. Biernacki, C. Lion, H. Kong, Opt. Lett. 12 (1987) 1029.
[4] C.-T. Chen, D.M. Kim, D. von der Linde, Appl. Phys. Lett. 34 (1979) 321.
[5] F. Mok, M. Tackitt, H.M. Stoll, Opt. Soc. Am. Tech. Dig. Ser. 12 (1989) 74.
[6] V.A. Fedorov, Yu.N. Korkishko, G. Lifante, F. Cussó, J. Eur. Ceram. Soc. 19 (1999) 1563.
[7] G. Lifante, E. Cantelar, J.A. Muñoz, R. Nevado, J.A. Sanz-García, F. Cussó, Opical Mateials. 13 (1999) 181.
[8] N. Iyi, K. Kitamura, F. Izumi, J.K. Yamamoto, T. Hayashi, H. Asano, S. Kimura, J. Solid State Chem. 101 (1992) 340.
[9] N. Iyi, K. Kitamura, Y. Yajima, S. Kimura, J. Solid State Chem. 118 (1995) 148.
[10] X.J. Chen, D.S. Zhu, B. Li, T. Ling, Z.K. Wu, Opt. Lett. 26 (13) (2001) 998.
[11] X.J. Chen, B. Li, J.J. Xun, D.S. Zhu, S.H. Pan, Z.K. Wu, J. Appl. Phys. 90 (3) (2001) 1516.
[12] L. Galambos, S.S. Orlov, L. Hessenlink, Y. Furukawa, K. Kitamura, S. Takekawa, J. Cryst. Growth 229 (2001) 228.
[13] Y. Furukawa, K. Kitamura, S. Takekawa, K. Niwa, Y. Yajima, N. Iyi, I. Mnushkina, P. Guggenheim, J.M. Martin, J. Cryst. Growth 211 (2001) 230.
[14] Y. Furukawa, K. Kitamura, S. Takekawa, K. Niwa, H. Hatano, Opt. Lett. 23 (1998) 1892.
[15] A. Ashkin, G.D. Boyd, J.M. Dziedzik, R.G. Smith, A.A. Ballman, K. Nassasu, Appl. Phys. Lett. 9 (1966) 72.
[16] G.G. Zhong, J. Jian, Z.K. Wu, in: Proceedings of the 11th International Quantum Electronics Conference, IEEE Cat. No. 80, CH 61-0, June 1980, p. 631.
[17] T.R. Volk, V.I. Pryalkin, N.M. Rubinina, Opt. Lett. 15 (18) (1990) 996.
[18] T.R. Volk, N.M. Rubinina, Ferroelect. Lett. 14 (1992) 37.
[19] J.K. Yamanoto, K. Kitamura, N. Iyi, S. Kimura, Y. Furukawa, M. Sato, Appl. Phys. Lett. 61 (1992) 2156.
[20] P.F. Bordui, R.G. Norwood, D.H. Jundt, M.M. Fejer, J. Appl. Phys. 71 (1992) 875.
[21] Y. FuruKawa, K. Kitamura, S. Takekawa, K.K. Niwa, Y. Yajima, N. Iyi, I. Mnushkina, P. Guggenheim, J.M. Martin, J. Cryst. Growth 211 (2000) 230.
[22] T. Volk, N. Rubinina, M. Wohlecke, J. Opt. Soc. Am. B 11 (9) (1994) 1681.
[23] H. Guenther, G. Macfarlane, Y. Furukawa, K. Kitamura, R. Neurgaonkar, Appl. Opt. 37 (32) (1998) 7611.
[24] O.F. Schirmer, O. Thiemanm, M. Wohlecke, J. Phys. Chem. Sol. 52 (1991) 185.
[25] R. Wang, W.S. Xu, X.R. Liu, J.Y. Wang, Chin. High Technol. Lett. 7 (2001) 92.
[26] R. Wang, Y.H. Xu, Y.D. Wei, Chin. Acta Photonic Sin. 30 (2001) 1307.